RSC Advances

ROYAL SOCIETY OF CHEMISTRY

www.rsc.org/advances

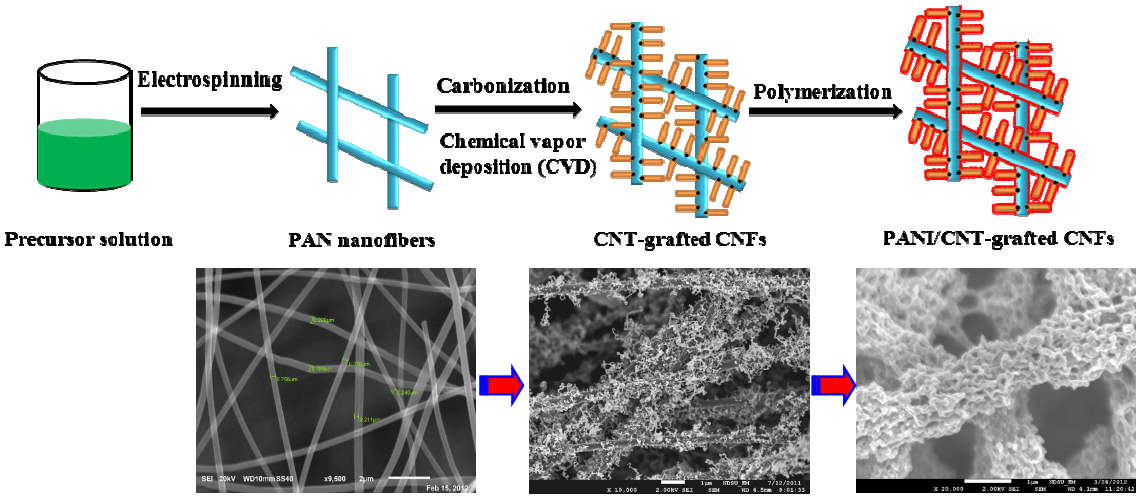

Electrospun carbon nanofibers surface-grown with carbon nanotubes and polyaniline for use as high-performance electrode materials of supercapacitors

Zhengping Zhou[a], Xiang-Fa Wu[a,*], and Haoqing Hou[b]

[a] *Department of Mechanical Engineering, North Dakota State University, Fargo, North Dakota 58108, USA*

[b] *College of Chemistry and Chemical Engineering, Jiangxi Normal University, Nanchang, Jiangxi 330027, China*

Abstract

This paper reports the synthesis and electrochemical performance of carbon nanofibers (CNFs) surface-grown with carbon nanotubes (CNTs) and nanostructured polyaniline (PANI) films, i.e., PANI/CNT/CNF, for use as a high-performance electrode material of pseudosupercapacitors. The PANI/CNT/CNF films were synthesized via *in situ* polymerization of aniline onto the surface of CNT-coated CNFs. The CNT-coated CNFs were prepared *via* electrospinning continuous polyacrylonitrile (PAN) nanofibers, followed by controlled carbonization and CNT growth. The morphology and microstructure of the PANI/CNT/CNF were characterized by means of scanning electron microscopy (SEM), transmission electron microscopy (TEM), and Raman spectroscopy. The electrochemical properties of the novel nanofiber films were characterized by electrochemical impedance spectroscopy (EIS), cyclic voltammetry (CV), and galvanostatic charge/discharge (GCD) in a 1 M aqueous H_2SO_4 solution as electrolyte. This unique porous nanofibrous structure exhibited the low equivalent series resistance (ESR) and interfacial charge-transfer resistance (R_{ct}) of 1.46 Ω and 0.55 Ω, respectively. Supercapacitors based on the present PANI/CNT/CNF electrodes behaved a high specific capacitance of ~503 F g^{-1} at a current density of 0.3 A g^{-1} and ~471 F g^{-1} (only 6% decrease) at 3 A g^{-1}. The maximum energy and power densities of ~70 W h kg^{-1} and ~15 kW kg^{-1} were achieved. In addition, over 92% of the initial capacitance was retained after

* Corresponding author. (Fax: +1-701-231-8913)
E-mail: xiangfa.wu@ndsu.edu (X.-F. Wu)

1000 charge/discharge cycles at a current density of 15 A g^{-1}. The results of the present experimental study suggested that such a unique multifunctional nanofibrous material can be utilized for developing high-performance electrochemical energy storage devices such as pseudosupercapacitors, battery-supercapacitor hybrids, etc.

Keywords: carbon nanofibers; carbon nanotubes; electrospinning; polyaniline; supercapacitor

1. Introduction

Energy consumption and production based on combustion of fossil fuels is deemed to have a severe future impact on the world's economy and ecology due to the decreasing availability of fossil fuels, growing environmental pollution, and global warming effects of greenhouse gas emissions. Future generations will become more and more relying on clean, sustainable and renewable energy resources such as solar, wind, and biomass based energies. Novel technologies and devices are desired to meet the urgent demand of energy harvesting, conversion, and storage. In parallel, there are worldwide interests and huge market potential in portable electronics and power tools, all-electric and plug-in hybrid electric vehicles (HEVs), and smart electrical grid integrated with fluctuating energy resources, e.g., solar and wind energies. These applications require low-cost, reliable and high-efficiency energy conversion and storage devices with high energy and power densities. Among a variety of electrochemical energy storage devices, electrical double layer capacitors (EDLCs), also called ultracapacitors or supercapacitors, have been under extensive investigation due to their high power density, ultrafast charge/discharge rates and long life cycles.[1-3] It has been generally accepted that supercapacitors can be designed to bridge the gap between rechargeable batteries and standard capacitors used in broad industrial sectors.[4] Yet, owing to their unique charge-storage mechanism of rooting charges at the interface of electrochemical double layers, supercapacitors usually carry a much lower energy density than that of secondary batteries (~1/100-1/10). Thus, it is technically crucial to enhance the energy density of supercapacitors while maintaining their existing advantages *via* nurturing novel charge-storage strategies, formulating innovative system

architectures, and synthesizing new generation high-performance electrode materials, electrolytes, and separators to meet the ever growing requirements of future systems.[5,6]

Furthermore, conducting polymers have been under intensive research as potential low-cost electrode materials for use in supercapacitors due to their capability of storing charges in the bulk state via a redox reaction and resulting high energy density.[4] As a promising conducting polymer for use in electrodes, polyaniline (PANI) has a high theoretical specific pseudocapacitance up to 750 F g^{-1}.[4,7] In addition, PANI exhibits other favorable properties such as low mass density and cost compared to broad transition-metal oxides (e.g., RuO_2, MnO_2, etc.), good electrical conductivity, and sound environmental stability.[8] However, several outstanding issues need to be resolved in rendering PANI as an electrode material to meet the practical requirements of supercapacitors such as the redox switching, relatively low electrical conductivity, and poor cyclability. These issues influence the pseudocapacitive performance of PANI supercapacitors.[8,9] To address these issues, PANI nanostructures have been grown on the surface of various carbon materials such as carbon nanotubes (CNTs), carbon nanofibers (CNFs), porous carbon, and graphene for use in supercapacitors.[10-15] For example, Zhou et al. reported a supercapacitor based on PANI-coated single-walled carbon nanotubes (SWCNTs) with a specific capacitance of 190.6 F g^{-1}.[16] Meng et al. produced a flexible PANI-coated paper-like buckypaper exhibited a capacitance up to 424 F g^{-1} with a retention ratio of 89.4% after 1000 cycles at 1 A g^{-1}.[17] Niu et al. developed ultrathin flexible SWCNT/PANI hybrid films with unique continuous "skeleton/skin" structure and this type of supercapacitor has a high energy and power densities of 131 W h kg^{-1} and 62.5 kW kg^{-1}, respectively.[18] Wei et al. fabricated novel CNFs surface-grown with whisker-like PANI nanorods, which exhibited a maximum specific capacitance of 427 F g^{-1} in 1 M aqueous H_2SO_4 solution as electrolyte.[19] Luo et al. also developed porous $ZnCo_2O_4$ nanotubes and carbon-coated MoO_2 nanofibers as high-performance electrode materials by using a low-cost single-nozzle electrospinning.[20,21]

The present paper, we report a simple rational synthesis route for fabricating a high-performance electrode material for use in supercapacitor based on electrospun CNFs surface-grown with CNTs and ultrathin PANI layers, coined as PANI/CNT/CNF. This synthesis route is illustrated in Fig. 1, which is

made up with three sequential processes, i.e., the "top-down" electrospinning for the precursor polymer nanofibers followed by controlled carbonization, "bottom-up" chemical vapor deposition (CVD), and *in situ* polymerization. First, the precursor solution was prepared by dissolved nickel (II) acetylacetonate [$Ni(AcAc)_2$] and polyacrylonitrile (PAN) powders in *N,N*-dimethylformamide (DMF) and electrospun to PAN/$Ni(AcAc)_2$ nanofibers with the diameter in the range of 200 to 300 nm.[22,23] These nanofibers were carbonized into continuous CNFs and then surfaced-grown with CNTs. During the CVD process of CNT growth, ethylene (C_2H_4) was used as carbon source, and Ni nanoparticles were employed as catalyst.[22] Consequently, PANI/CNT/CNF films were synthesized by *in situ* polymerization of anilines on the CNT/CNF networks which acted as a porous scaffold for active sites of anilines resulted in ternary hierarchical nanofibrous material with ultrathin PANI layers.

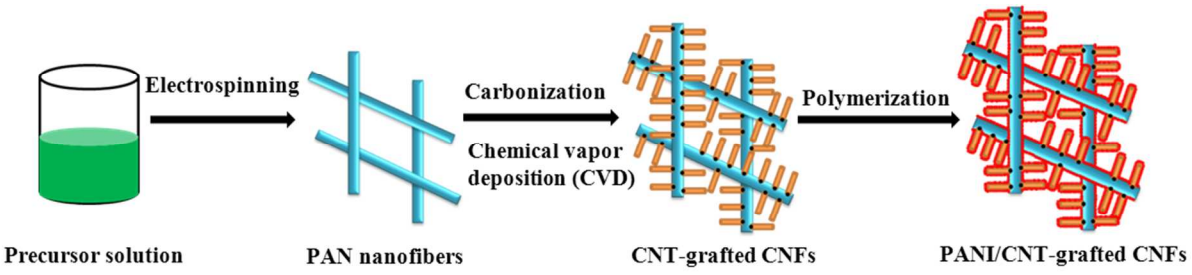

Fig. 1. Schematic rational synthesis route for fabricating ultrathin PANI layers based on CNT/CNF template.

The proposed PANI/CNT/CNF films exhibited several unique features favorable for high-performance supercapacitors, which include: 1) the ultrathin PANI layers deposited onto CNT/CNF networks enable the fast electron transport and effective current collection;[6,24] 2) the CNF network served as current collector and the CNTs on CNF surface functioned as short channels to bridge the PANI layers, which ensures the high rate charge/discharge capability;[13,24,25] and 3) the ultrathin PANI layers carried very high specific surface area and complex surface morphology beneficial to the large specific pseudocapacitance and high energy and power densities. The layout of the rest of the paper is the follows.

Section 2 is the experimental part to detail processes for fabrication of the proposed PANI/CNT/CNF films and electrochemical measurements. Section 3 is to present detailed experimental results and discussion on the experimental data. The concluding remarks of the paper research are made in Section 4.

2. Experimental

2.1 Materials

Polyacrylonitrile (PAN, Mw=150,000) powders, nickel (II) acetylacetonate [$Ni(AcAc)_2$], *N,N*-dimethylformamide (DMF, 99%), ammonium persulfate (APS), sulfuric acid (H_2SO_4), and aniline monomer were purchased from Sigma-Aldrich Chemical Co. (St. Louis, MO, USA). All the chemicals were used as received without further purification or modification.

2.2 Synthesis of CNT/CNF films

The precursor $Ni(AcAc)_2$/PAN (mass ratio 2:5) nanofiber films were fabricated by means of the low-cost electrospinning technique. During this process, PAN and $Ni(AcAc)_2$ powders were first dissolved in DMF to form a 10 wt.% electrospinnable solution, which was then placed into a 10-ml plastic syringe installed with a stainless steel spinneret. Electrospinning was performed in a DC electric field of 90 kV m^{-1}, which was generated by applying a positive 18 kV voltage to a 20 cm gap between the spinneret and nanofiber collector.

Stabilization and carbonization of the films were performed in a tubular quartz furnace. The films were first annealed at 215 °C for 1h in air for oxidative stabilization, followed by heating up to 500 °C at a rate of 5 °C min^{-1} in Ar. Subsequently, the films were annealed at 500 °C in a mixed H_2/Ar flow for 1h to reduce Ni^{2+} to Ni atom. The Ni atoms were then grown on the CNF surface with the catalytic nanoparticles in shape. These Ni nanoparticles functioned as catalysts to decompose the hydrocarbon molecules into carbon atoms. The Ni/CNF films were heated up to 900 °C at a rate of 5 °C m^{-1} and annealed for 30 min in Ar flow for full carbonization. After that, the furnace was cooled down to 650°C in Ar and maintained at this temperature for 1h to grow CNTs *via* introducing a mixture flow of Ar/C_2H_4.

2.3 Preparation of the PANI/CNT/CNF film

The PANI/CNT/CNF films were synthesized by *in situ* polymerization of aniline onto the CNT/CNF films as templates. A solution of 0.03 M aniline in 200 ml 1 M H_2SO_4 was first prepared. The CNT/CNF films were immersed in the solution for 1 h. Then, another 200 ml 1 M H_2SO_4 solution containing 0.0075 M APS was added into the above solution, drop-by-drop. The mixture solution was continuously stirred for 5 h and the aniline polymerized in an ice-bath. The molar ratio of aniline/APS was 4:1. During this period, the color of the solution slowly changed until dark green. After polymerization, the PANI/CNT/CNF films were filtered and washed sequentially with deionized water and acetone. Then, the films were dried in a vacuum at 70 °C for 3 h. The PANI content in the PANI/CNT/CNF films was ~50% by weight.

2.4 Structural and Electrochemical Characterization

The surface morphology and structure of the films were analyzed by a high-resolution field-emission scanning electron microscope (SEM, JEOL JSM-7600F), transmission electron microscope (TEM, JEOL JEM-2100), and Raman spectroscope (Nicolet NXR 9650 FT-Raman spectrometer, 632.8 nm). The electrochemical properties of the supercapacitor cells were characterized by electrochemical impedance spectroscopy (EIS), cyclic voltammetry (CV), and galvanostatic charge/discharge (GCD). The three-electrode electrochemical impedance spectroscopy (EIS) setup was employed for the impedance measurements in this study. A saturated calomel electrode was used as the reference electrode. 1 M H_2SO_4 aqueous solution and stainless steel wire mesh were used as the electrolyte and the current collector, respectively. EIS was tested in the frequency range of 10^5-0.01 Hz by Electrochemical Multiplexer ECM8 (Gamry Instruments, Inc., PA). The CV and GCD were conducted by Arbin BT-2000 testing system (Arbin Instruments, TX) in a 1 M H_2SO_4 electrolyte within a voltage range of -0.2 to 0.8 V. The specific capacitance, energy density, and power density were calculated by conducting GCD curves with constant current densities. The specific capacitance, C_S (F g^{-1}), energy density, E_d (W h kg^{-1}) and power density, P_d (kW kg^{-1}), delivered

by supercapacitors are determinate experimentally according to the following relations:[18]

$$C_s = 2\frac{I\times\Delta t}{M\times\Delta V} \quad (1)$$

$$E_d = \frac{1}{2}C_s\Delta V^2 \quad (2)$$

$$P_d = \frac{E_d}{\Delta t} \quad (3)$$

where I is the constant charge/discharge current (A), Δt the discharge time (s), ΔV the potential difference (V) during the discharge/discharge process, and M is the average mass (g) of two electrodes.

3. Results and Discussion

Figures 2(A) and (B) show the typical SEM micrographs of the CNF and CNT/CNF films synthesized in the present study, respectively. The CNFs have a smooth surface with a nearly uniform diameter in the range of 200 to 300 nm. From Fig. 2(C), the entangled CNTs with the diameter of 20-30 nm were randomly grown on the surface of CNFs. The length of CNTs was about a few microns. The diameter and length of the CNTs can be tailored by adjusting the material and process parameters such as the catalyst, carbon sources, temperature, and the duration of the CVD.[22,26] It can be observed that the connection of CNT/CNF between CNFs and CNTs is interconnected, continuous, and not overlapping (as shown in Fig. 2(D)). Compared with the purified CNFs or CNTs, the unique porous CNT/CNF films are expected to have the advantages in transporting electrons over a large specific surface area. Furthermore, the CNT/CNF also plays an important role in reducing CNT agglomeration in aqueous solution. These results expected that the porous CNT/CNF films could act as good templates for the formation of the PANI/CNT/CNF films.

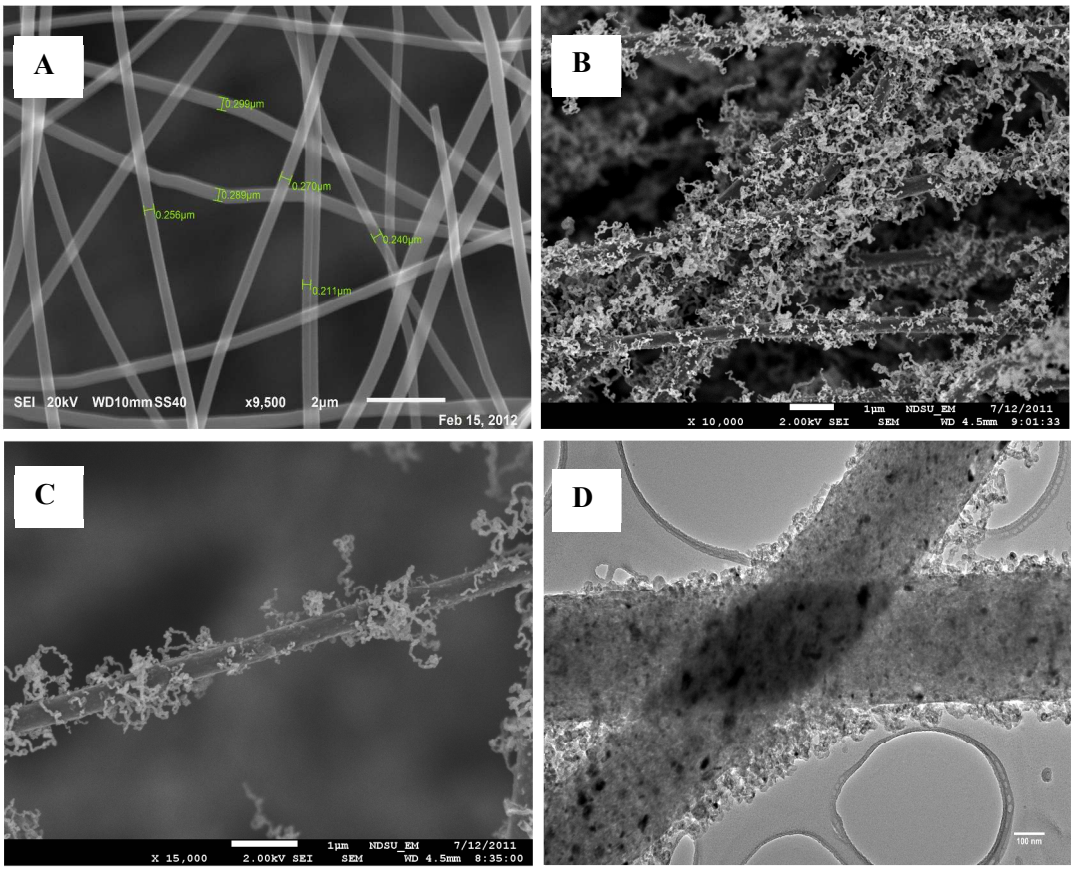

Fig. 2. (A)-(C): SEM micrographs of purified CNFs, CNT/CNFs, and a typical CNT-grown CNF, respectively; (D): TEM image of CNT/CNFs.

It is known that the morphology and microstructure of PANI can be adjusted by templates during *in situ* polymerization.[18] In this process, CNF and CNT/CNF films were used as 3D free-standing templates for generating ordered PANI nanostructures. Due to the hydrogen bond effect of CNFs, some aniline molecules may be adsorbed on the surface of CNFs.[27] With addition of APS, these adsorbed aniline molecules polymerized preferentially to form tiny PANI 'seeding dots' (quantum dots). These tiny "seeding dots" further reacted to form PANI nanowires as shown in Fig. 3(A).[19,27] The obtained PANI nanowires were needle-like in morphology and vertically arrayed on the surface of CNFs. Figure 3 (B) further reveals the formation of uniform needle-like PANI nanowires which have the diameter ranging

from 50 to 80 nm and the height up to 150 nm. In addition, the diameter and height of the PANI nanowires could be tuned via adjusting the concentration of aniline, temperature, and duration of polymerization.[14,19,27]

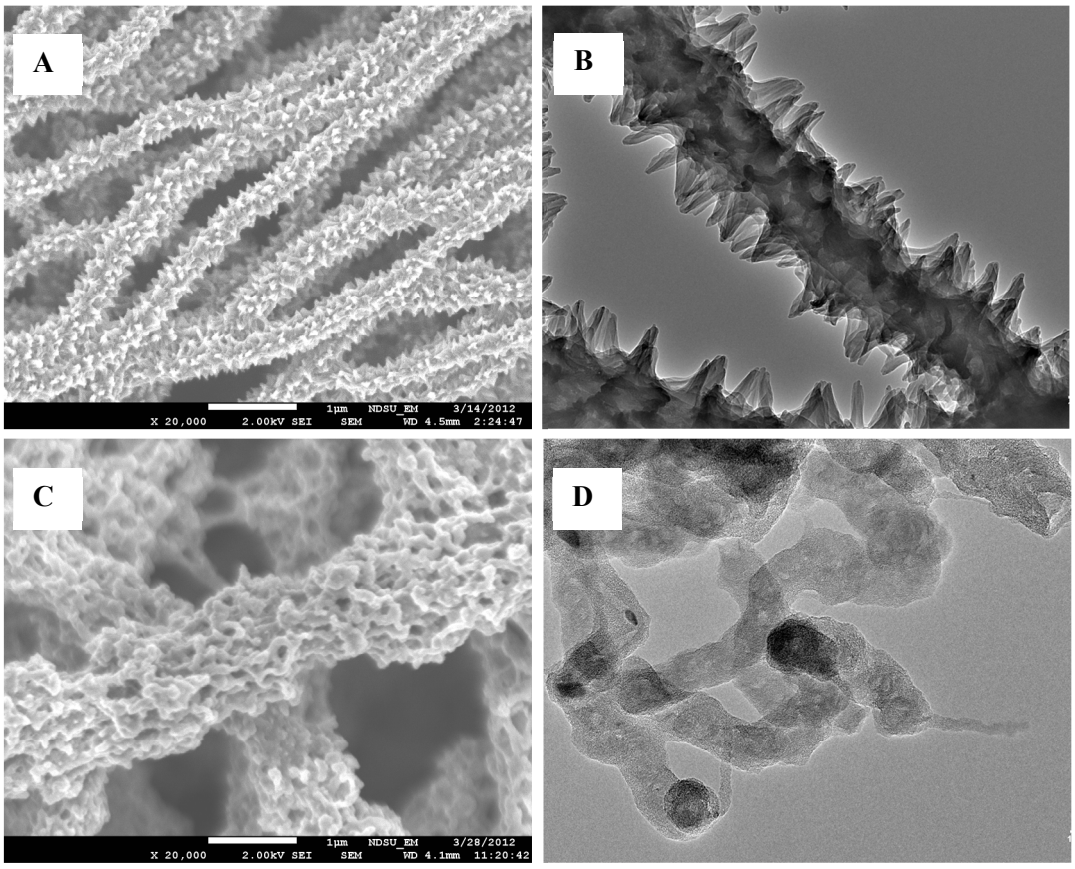

Fig. 3. (A) and (C): SEM micrographs of PANI/CNF and PANI/CNT/CNF, respectively; (B) and (D): TEM images of PANI/CNF and PANI/CNT/CNF, respectively.

Figure 3(C) shows the SEM image of PANI-coated CNT/CNF films, which have homogenous and ultrathin PANI layers on their surface. However, the needle-like PANI nanowires on the surface PANI/CNF films were not observed in this SEM analysis. This is because the anilines were sufficiently adsorbed on the surface of CNT/CNF films to form a thin PANI layer at the initial stage of

polymerization, owing mainly to the rich hydroxyl and carbonyl groups coexisting on the surface of CNT whiskers as well as its high aspect ratio.[15,28] PANI multi-layers were further formed via reaction of the as-formed PANI with the free aniline in solution. The TEM micrograph as shown in Fig. 3D clearly validates the successful synthesis of PANI/CNT/CNF films. It is can be detected that the diameters of PANI/CNT nanowires were about 30-60 nm, while the thickness of PANI layers on the surface of CNTs was about 10-30 nm. Compared to those nanostructured PANI that was synthesized with the aid of CNTs as reported in the literature,[10,15,28,29] the present PANI/CNT/CNF films provided a rougher surface with high specific surface area to achieve the unique porous nanostructures of PANI. Meanwhile, the CNT/CNF networks were functioned as the excellent current-delivery channels to suppress the electrical contact resistance of the electrodes due to their high electrical conductivity and excellent topological connectivity.

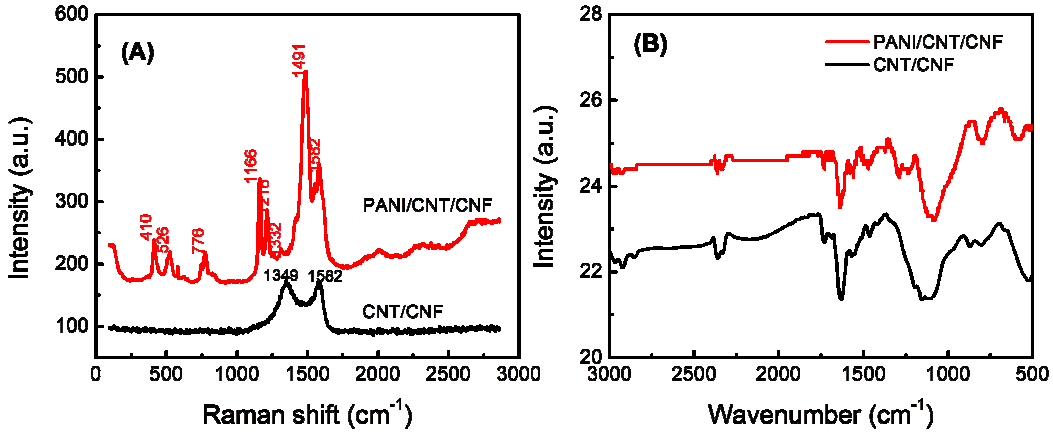

Fig. 4. (A): Raman spectra of CNT/CNF and PANI/CNT/CNF films; (B): FTIR spectra of CNT/CNF and PANI/CNT/CNF films.

The chemical microstructures of electrode materials were characterized by means of Raman spectroscopy, which can provide detailed information of their molecular structure to further confirm the PANI/CNT/CNF. The Raman spectra of PANI/CNT/CNF and CNT/CNF films were carried out at an

excitation wavelength of 632.8 nm as shown in Fig. 4 (A). The curve of CNT/CNF film shows two typical characteristic peaks at 1,582 cm^{-1} (G bands) and 1,349 cm^{-1} (D bands), which are attributed to the phonons propagating along the graphitic structures and the disordered turbostratic structures or defects, respectively.[23] In the plot of the PANI/CNT/CNF films, it can be observed the characteristic bands of PANI and some overlap bands with CNT/CNF films. The band located at 1,166 cm^{-1} was attributed to the C-H bending vibration of the benzenoid/quinoid ring; the peak located at 1,216 cm^{-1} was correlated to the weak C-N stretching. The bands situated at 1,491 cm^{-1} and 1,582 cm^{-1} were corresponded to the C=N stretching of the quinoid ring and C-C stretching of the benzenoid ring of PANI, respectively. [10,19,31] Moreover, the peak of $C\text{-}N^{*+}$ at 1,333 cm^{-1} was resulted from the formation of a radical cation on the doping and co-doping of PANI.[10] As shown, the PANI/CNT/CNF films presented similar Raman data with the PANI materials prepared by polymerization under acid conditions, in good agreement with several earlier works.[15,19,28, 29] Figure 4(B) shows the typical FTIR spectrum of PANI/CNT/CNF and CNT/CNF films. The absorption peaks at 1,564 cm^{-1} and 1,465 cm^{-1} correspond to the C–C stretching deformation mode of the quinoid (Q) and benzenoid (N) rings of PANI, respectively.[32] The peak at 3,420 cm^{-1} is due to the N-H stretching vibration of PANI, while the peaks at 1,231 cm^{-1} and 1,294 cm^{-1} are attributed to the C-N stretching vibration of an aromatic conjugation. The N-Q-N stretching band at 1,087 cm^{-1} is the characteristic band of the PANI salt.[33] The intensities of these peaks imply the formation of PANI layers onto the surface of CNT/CNFs. In contrast, a characteristic band of CNT/CNFs associated with C-C symmetric stretching was observed at 790 cm^{-1}.

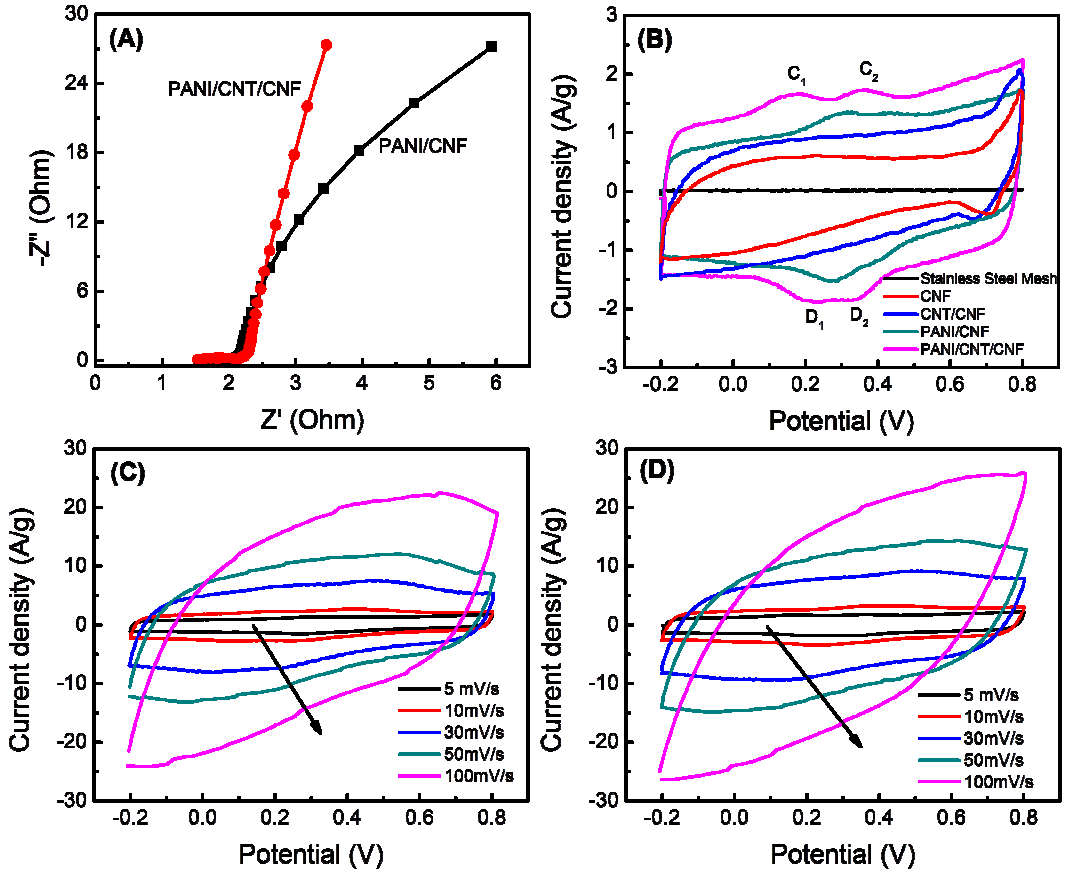

Fig. 5. (A): Nyquist plots of PANI/CNF and PANI/CNT/CNF film electrodes; (B): CV curves of stainless steel mesh, CNF, CNT/CNF, PANI/CNF and PANI/CNT/CNF film electrodes at a scan rate of 5 mV s^{-1}; (C) and (D): CV curves of PANI/CNF and PANI/CNT/CNF film electrodes at varying scan rates, respectively.

Electrochemical impedance spectroscopy (EIS) has been considered as a very effective method for analyzing the electrochemical impedance properties including the internal resistance, charge transport in electrode/electrolyte, and ion diffusion of electrochemical devices.[30] In this work, the stainless steel mesh was used as the current collectors and a 1 M H_2SO_4 aqueous solution was utilized as the electrolyte. Figure 5(A) shows the Nyquist plots of PANI/CNF and PANI/CNT/CNF film electrodes in the frequency ranging from 0.01Hz to 100 kHz under open circuit potential. As shown, both Nyquist plots consist of

two distinct parts including a distorted semicircle at the high frequency region and a sloped line in the low frequency region. The *x*-intercept in the Nyquist plots represents the equivalent series resistance (ESR), which is corresponded to the electrolyte solution resistance and the contact resistance across the electrode/electrolyte interface. As observed from these plots, the ESR values of PANI/CNF and PANI/CNT/CNF electrodes are about 1.50 and 1.46 Ω, respectively. As a result, these electrodes have a small semicircle in the high frequency region, corresponding to a low interfacial charge-transfer resistance (R_{ct}). Estimate of the diameter of semicircles show that the R_{ct} values are 0.50 and 0.55 Ω, respectively. Such a low R_{ct} was resulted from the good interfacial conductivity between the PANI and carbon materials. Besides, the R_{ct} values of both the PANI/CNF and PANI/CNT/CNF electrodes are much less than those reported for PANI/CNF composite paper (9.2 Ω),[27] PANI-CNT/Ni hybrid electrode (10.0 Ω),[31] and ordered mesoporous PANI/carbon composite (5.4 Ω).[34] The inclined lines of the Nyquist plots were due to the ion diffusion in the electrode/electrolyte, known as the Warburg behavior.[35] The PANI/CNT/CNF electrode with nearly vertical line exhibited the higher accessibility of PANI surfaces for ion diffusion than that of PANI/CNF electrode. This is mostly due to the unique integrated nanostructures, in which the CNF network functioned as a current collector and CNT-coated CNFs acted as conductive channels to connect the PANI layers. All EIS data therein demonstrated the successful synthesis of PANI/CNT/CNF hybrids with enhanced ion diffusivity and conductivity.

The electrochemical properties of the synthesized electrode materials were characterized by CV and GCD in this study. Fig. 5(B) shows the CV curves of the resulting supercapacitors. The experiments were carried out at a potential scan rate of 5 mV s^{-1} in a wide potential range of -0.2 - 0.8 V. The background signal of the stainless steel mesh is negligible. Compared to the purely CNF electrode, the CV curve of the CNT/CNF electrode exhibited a nearly rectangular shape within the time-potential plot, which indicates its pure double-layer electrochemical performance. Such observation is due mostly to the unique structure of CNT/CNFs with enhanced specific surface area and conductivity. However, the PANI/CNF and PANI/CNT/CNF electrodes clearly demonstrated typical two pairs of redox peaks (C_1/D_1 and C_2/D_2) as shown in Fig. 5(B), which are the characteristic of PANI involved in the electrochemical reactions. The

first pair of peaks C_1/D_1 is ascribed to the redox transition from the leucoemeraldine form to polaronic emeraldine form. The second pair of peaks C_2/D_2 is corresponded to the Faradaic transformation of emeraldine/pernigraniline.[15,19,35] Generally speaking, conducting polymer (e.g., PANI and PPy) store and release charges through redox transitions, which are associated with the π–conjugated polymer chains. During the oxidation process (also referred to as *p*-doping), electrolyte ions are transferred to the polymer surface. In contrast, when the reduction process (also known as un-doping), electrolyte ions are released back into the solution. As expected, the current density of PANI/CNT/CNF electrode was much higher than that of the CNF, CNT/CNF, and PANI/CNF electrode at the same scan rate, implying an improved electrochemical capacity of PANI/CNT/CNF film. In addition, the CV plot of the PANI/CNT/CNF electrode carries a shape different from that PANI/CNF and it even has a larger enclosed area, which indicates that PANI/CNT/CNF electrode exhibits a significant synergistic effect exists between the PANI layer and CNT/CNF network. Figures 5(C) and (D) present the CV curves of PANI/CNF and PANI/CNT/CNF film electrodes at varying scan rates from 5 to 100 mV/s, respectively. An obvious increase of the current densities can be detected for these electrodes. Meanwhile, it is notable that the cathodic peaks shifted positively, while the anodic peaks shifted negatively, which is attributed mainly to a slight increase of electrode resistance at high scan rates.[12] The redox peaks even disappeared at the scan rate of 100 mV/s, and the CV curves exhibit a symmetric and approximately rectangular shape, which indicates the excellent charge propagation and low contact resistance in the electrodes.[15,36,37]

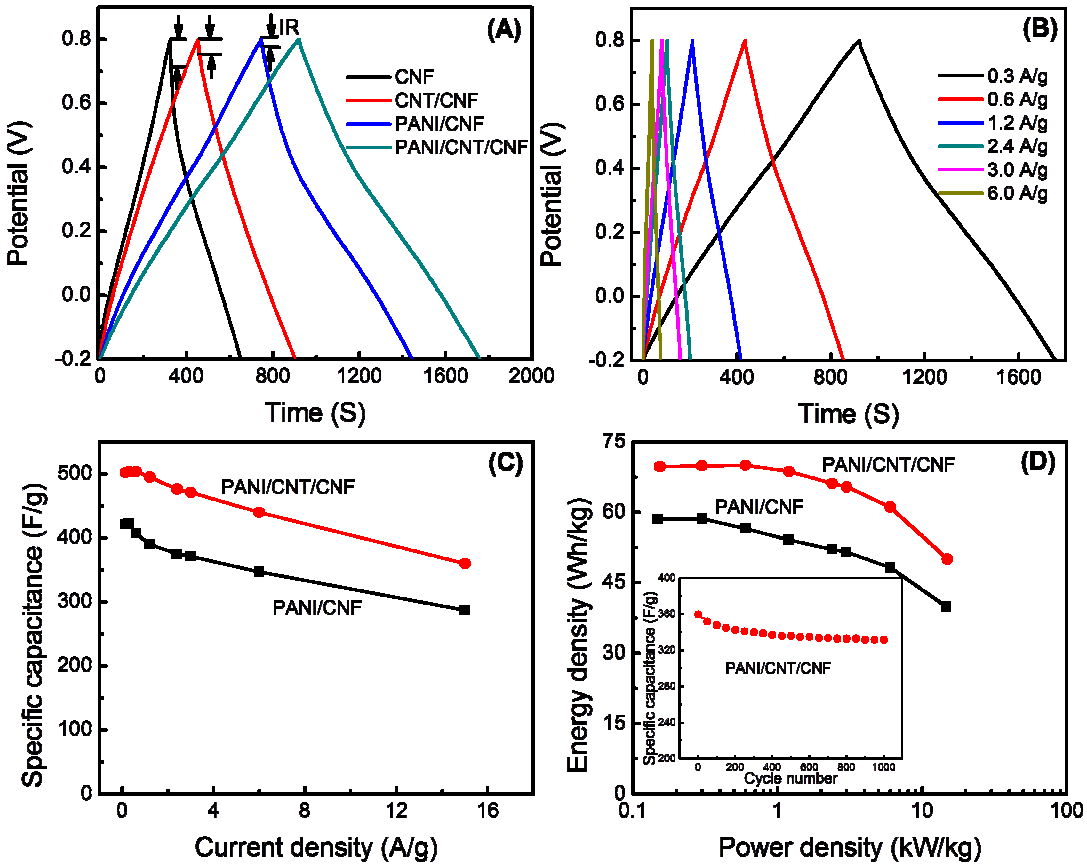

Fig. 6. (A): GCD curves of CNF, CNT/CNF, PANI/CNF, and PANI/CNT/CNF film electrodes at a current density of 0.3 A g^{-1}, respectively; (B): GCD curves of PANI/CNT/CNF film electrodes at different current densities; (C): Specific capacitance *vs.* current density for PANI/CNF and PANI/CNT/CNF film electrodes; (D): Charging/discharging cycling stability of PANI/CNT/CNF film electrodes at a current density 15 A g^{-1}.

To further quantify the specific capacitance of the electrodes, GCD tests of capacitor cells were performed in 1 M H_2SO_4 aqueous solution. Figure 6(A) shows the GCD curves of CNF, CNT/CNF, PANI/CNF, and PANI/CNT/CNF film electrodes at a current density of 0.3 A g^{-1}, respectively. In the case of CNF electrode, the GCD curve deviates from the triangular shape during discharging, whereas in

the case of CNT/CNF electrode, the GCD curve is nearly a triangular shape, indicating the reversible charge/discharge behavior of ideal EDLC.[5] The "IR drop" of CNT/CNF electrode is lower than that of the CNF electrode, which demonstrated that the internal resistance of the CNT/CNF electrode has been greatly suppressed by the grown CNTs. The GCD curves of PANI/CNF and PANI/CNT/CNF electrodes deviate from the linear shape owing to the faradic pseudocapacitive effect of PANI.[38,39] Due to its high capacitance, the PANI/CNT/CNF electrode exhibited a delayed discharge time duration compared to PANI/CNF electrode. Such high capacitance also confirmed the existence of the synergistic effect in PANI/CNT/CNFs. It is worth to mention that the "IR" drops of PANI/CNT/CNF and PANI/CNF electrodes are lower than that of CNT/CNF and pure CNF electrodes, which might be relevant to their low ion diffusion/transport resistance at the PANI surface.

The specific capacitance was calculated from the GCD curves according to relation (1). At a current density of 0.3 A g^{-1}, the specific capacitance of PANI/CNT/CNF electrode is 503 F g^{-1}, higher than that of PANI/CNF (422 F g^{-1}), CNT/CNF (270 F g^{-1}), and CNF (196 F g^{-1}) electrodes. These results show that CNTs coated onto CNFs noticeably enhanced the specific surface area of CNFs and thus the specific capacitance, and CVD-based PANI deposition onto the surface of CNTs and CNFs further triggered the favorable pseudocapacitive effect, which greatly increased the specific capacitance of the resulting electrode material. As a result, it can be concluded that the enhanced capacitance in PANI/CNT/CNF electrode material is due mainly to the synergetic effect of the ultrathin PANI layers on unique CNT/CNF network. In this study, PANI is about 50 wt.% of the CNT/CNFs. To estimate the synergistic effect between ultrathin PANI layers and CNT/CNFs, the specific capacitance of the ultrathin PANI layers in this case can be calculated is 736 F g^{-1}, i.e., [(503 F g^{-1} (PANI/CNT/CNF) − 270 F g^{-1} (CNT/CNF)*50%] / 50%}, which is 2.25 – 4.35 times that of pure PANI nanofiber electrodes (169-326 F g^{-1}).[9,14,40] The capacitance of the present PANI/CNT/CNF electrode is competitive with those of many recently reported supercapacitors, e.g., PANI/SWCNT-based composite cloth (410 F g^{-1} at 0.5 A g^{-1}),[18] graphene/CNT-PANI composite (271 F g^{-1} at 0.3 A g^{-1}),[36] PANI/MWCNT nanofiber (490 F g^{-1} at 0.5 A g^{-1}),[15] PANI/MWCNT composite (560 F g^{-1} at 1 mV s^{-1}),[41] CNT/PANI composite (424 F g^{-1} at 0.1 A g^{-1}),[26]

PANI-CNT composite (528 F g^{-1} at 1.0 A g^{-1}),[11] core-shell MWCNT /graphene oxide nanoribbon (252.4 F g^{-1} at 50 mV s^{-1}) [42], and SWCNT/BiVO4 composite (395 F^{-1} g at 2.5 A g^{-1})[43].

The present GCD curves of the PANI/CNT/CNF electrodes were examined at different current densities from 0.3 to 6.0 A g^{-1} as shown in Fig. 6(B). It can be observed that all the curves are nearly linear and symmetrical in shape, which indicates that the supercapacitor carries an excellent electrochemical reversibility in a wide range of current density. Figure 6(C) shows the influence of the specific capacitance of PANI/CNF and PANI/CNT/CNF electrodes upon the current densities. Interestingly, the capacitance values slightly increased at the low current densities and then decreased. For example, the values of capacitance of the PANI/CNT/CNF electrode are 502, 503, and 504 F g^{-1} at the current densities of 0.15, 0.3, and 0.6 A g^{-1}, respectively, which demonstrate the superior rate capability. When the current density is increased to 3 A g^{-1}, the capacitance of PANI/CNT/CNF can be still maintained as high as 471 F g^{-1}, only 6% decrease compared to the capacitance at 0.3 A g^{-1}. On the contrary, up to 13% of the capacitance was decayed for the PANI/CNF electrode. Besides, about 28% decrease of the maximum capacitance of PANI/CNT/CNF electrode was found even at a high current density up to 15 A g^{-1}.

To evaluate the cycling capability of PANI/CNT/CNF supercapacitor, the GCD tests have been run for 1,000 cycles at a high current density of 15 A g^{-1} as shown in the inset of Fig. 6(D). The capacitance only dropped ~8% from 360 to 332 F g^{-1} after 1,000 cycles, which reveals the remarkable cycling stability of the PANI/CNT/CNF material to be used for high-performance electrochemical supercapacitors. Furthermore, the energy and power density values of supercapacitors were also calculated from the GCD curves at varying current densities. Figure 5(D) shows the Ragone plot of PANI/CNF and PANI/CNT/CNF supercapacitors. It can be found that the PANI/CNT/CNF supercapacitor delivered a high energy density of ~50 W h kg^{-1} at a high power density of ~15 kW kg^{-1}. This energy density is ~25% higher than that of the PANI/CNF supercapacitor. The highest energy density of ~70 W h kg^{-1} at a power density of 600 W kg^{-1} were obtained from the PANI/CNT/CNF supercapacitor, which is almost one order higher than the values from the commercial supercapacitors that have the energy density of 1-10 W h kg^{-}

[1,8]. It should be pointed out that these characteristics were performed at a potential window of -0.2 to 0.8 V in 1 M H_2SO_4 aqueous electrolyte. Therefore, we believe that the PANI/CNT/CNF material could be coupled with a suitable battery electrode material to form a battery-supercapacitor hybrid (BSH) to achieve the high performance in practical energy storage devices.

4. Conclusions

In summary, ordered and flexible PANI/CNT/CNF films have been successfully synthesized *via* three sequential steps: electrospinning, CNT growth, and *in situ* polymerization. The incorporation of the continuous CNT/CNF films has significantly enhanced the electrochemical properties of PANI/CNT/CNF film electrodes, such as the high interfacial charge-transfer conductivity and ion diffusivity. This is mostly due to their unique integrated nanostructure in which the CNF network functioned as a current collector and charge channel and the CNTs coated onto CNFs acted as short wires to connect the PANI layers. The supercapacitors based on porous PANI/CNT/CNF electrodes exhibited a high specific capacitance of 503 F g^{-1} at a current density of 0.3 A g^{-1} and a super cycling stability of ~92% specific capacitance retention over 1,000 cycles. A highest energy density of ~70 W h kg^{-1} and maximum power density of ~15 kW kg^{-1} have been obtained. Due to the strong synergistic effect between the PANI layers and CNT/CNF networks in this study, such high-performance porous electrode materials are expected for broad applications in electrochemical energy storage devices.

Acknowledgments

The support of the research by National Science Foundation (Award No.: CMMI-1234297) and DoE EPSCoR-Sustainable Energy Seed Grant Initiative Program (SUNRISE) (Award No.: DE-FG02-06ER46292, Seed Grant: FAR 0017563) is gratefully acknowledged. Z. Zheng thanks the North Dakota EPSCoR Doctoral Dissertation Fellowship Award.

References

[1] J. R. Miller, P. Simon, *Science*, 2008, **321**, 651.

[2] J. Chmiola, G. Yushin, Y. Gogotsi, C. Portet, P. Simon, P. L. Taberna, *Science*, 2006, **313**, 1760.

[3] P. Simon, Y. Gogotsi, *Nat. Mater.*, 2008, **7**, 845.

[4] G. A. Snooka, P. Kaob, A. S. Best, *J. Power Sources*, 2011, **196**, 1.

[5] Q. T. Qu, Y. S. Zhu, X. W. Gao, Y. P. Wu, *Adv. Energy. Mater.*, 2012, **8**, 950.

[6] X. L. Wang, G. Li, Z. Chen, V. Augustyn, X. M. Ma, G. Wang, B. Dunn, Y. F. Lu. *Adv. Energy Mater.*, 2011, **1**, 1089.

[7] K. Lota, V. Khomenko, E. Frackowiak, *J. Phys. Chem. Solids*, 2004, **65**, 295.

[8] X. Zhao, B. M. Sánchez, P. J. Dobson, P. S. Grant, *Nanoscale*, 2011, **3**, 839.

[9] Y. K. Zhou, B. L. He, W. J. Zhou, J. Huang, X. H. Li, B. Wu, H. L. Li, *Electrochim. Acta*, 2004, **49**, 257.

[10] D. Ghosh, S. Giri, A. Mandal, C. K. Das. *RSC Adv.*, 2013, **3**, 11676.

[11] W. Chen, R. B. Rakhi, H. N. Alshareef, *J. Mater. Chem. A*, 2013, **1**, 3315.

[12] Y. G. Wang, H. Q. Li, Y. Y. Xia, *Adv. Mater.*, 2006, **18**, 2619.

[13] C. Portert, G. Yushi, Y. Gogotsi, *J. Electrochem. Soc.*, 2008, **155**, A531.

[14] S. J. He, X. W. Hu, S. L. Chen, H. Hu, M. Hanif, H. Q. Hou, *J. Mater. Chem.*, 2012, **22**, 5114.

[15] S. P. Zhou, H. M. Zhang, X. H. Wang, J. Lia, F. S. Wang, *RSC Adv.*, 2013, **3**, 1797.

[16] Y. K. Zhou, B. L. He, W. J. Zhou, J. Huang, X. H. Li, B. Wu, H. L. Li, *Electrochim. Acta*, 2004, **49**, 257.

[17] C. Z. Meng, C. H. Liu, S. S. Fan, *Electrochem. Comm.*, 2009, **11**, 186.

[18] Z. Q. Niu, P. S. Luan, Q. Shao, H. B. Dong, J. Z. Li, J. Chen, D. Zhao, L. Cai, W. Y. Zhou, X. D. Chen, S. H. Xie, *Energy Environ. Sci.*, 2012, **5**, 8726.

[19] J. Y. Wei, J. N. Zhang, Y. Liu, G. H. Xu, Z. M. Chen, Q. Xu, *RSC Adv.*, 2013, **3**, 3957.

[20] W. Luo, X. Hu, Y. Sun, Y. Huang, *J. of Mater. Chem.*, 2012, **22**, 4910.

[21] W. Luo, X. Hu, Y. Sun, Y. Huang, *Phys. Chem. Chem. Phys.*, 2011, **13**, 16735. [22] Z. P. Zhou, X. F.

Wu, H. Fong, *Appl. Phys. Lett.* 2012, **100**, 023115.

[23] Z. P. Zhou, X. F. Wu, *J. Power Sources*, 2013, **222**, 410.

[24] X. F. Wu, Z. P. Zhou, W. M. Zhou, *Appl. Phys. Lett.*, 2012, **100**, 193115.

[25] Z. Chen, J. Wen, C. Z. Yan, L. Rice, H. S. Sohn, M. Q. Shen, M. Cai, B. Dunn, Y. F. Lu, *Adv. Energy Mater.*, 2011, **1**, 551.

[26] C. L. Lai, Q. H. Guo, X. F. Wu, D. H. Reneker, H.Q. Hou, *Nanotech.*, 2008, **19**, 1.

[27] X. B. Yan, Z. X. Tai, J. T. Chen, Q. J. Xue, *Nanoscale*, 2011, **3**, 212.

[28] C. Peng, J. Jin, G. Z. Chen, *Electrochim. Acta*, 2007, **53**, 525.

[29] M. N. Hyder, S. W. Lee, F. C. Cebeci, D. J. Schmidt, Y. S. Horn, P. T. Hammond, *ACS Nano*, 2011, **5**, 8552.

[30] R. Kötz, M. Carlen, *Electrochim. Acta*, 2000, **45**, 2483.

[31] Y. Li, Y. Z. Fang, H. Liu, X. M. Wu, Y. Lu, *Nanoscale*, 2012, **4**, 2867.

[32] Q. W. Tang, J. H. Wu, X. M. Sun, Q. H. Li, J. M. Lin, *Langmuir* 2009, **25**, 5253.

[33] D. S. Yuan, T. X. Zhou, S. L. Zhou, W. J. Zou, S. S. Mo, N. N. Xia, *Electrochem. Commun.* 2011, **13**, 242.

[34] L. X. Li, H. H. Song, Q. C. Zhang, J. Y. Yao, X. H. Chen, *J. Power Sources*, 2009, **187**, 268.

[35] D. W. Wang, F. Li, J. P. Zhao, W. C. Ren, Z. G. Chen, J. Tan, Z. S. Wu, I. Gentle, G. Q. Lu, H. M. Cheng, *ACS Nano*, 2009, **3**, 1745.

[36] Q. Cheng, J. Tang, N. Shinya, L. C. Qin, *J. Power Sources*, 2013, **241**, 423.

[37] Y. S. Luo, D. Z. Kong, Y. L. Jia, J. S. Luo, Y. Lu, D. Y. Zhang, K. W. Qiu, C. M. Li, T, Yu. *RSC Adv.*, 2013, **3**, 5851.

[38] S. Biswas, L. T. Drzal, *Chem. Mater.*, 2010, **22**, 5667.

[39] S. Li, Y. Luo, Wei Lv, W. J. Yu, S. D. Wu, P. X. Hou, Q. H. Yang, Q. B. Meng, C. Liu, H. M. Cheng, *Adv. Energy Mater.*, 2011, **1**, 486.

[40] M. K. Liu, Y.-E Miao, C. Zhang, W. W. Tjiu, Z. B. Yang, H. S. Peng, T. X. Liu, *Nanoscale*, 2013, **5**, 7312.

[41] Y. Zhou, Z. Y. Qin, L. Li, Y. Zhang, Y. L. Wei, L. F. Wang, M. F. Zhu, *Electrochim. Acta*, 2010, **55**,

3904.

[42] L. Y. Lin, M. H. Yeh, J. T. Tsai, Y. H. Huang, C. L. Sun, K. C. Ho, *J. Mater. Chem. A.* 2013, **1**, 11237.

[43] Z. Khan, S. Bhattu, S. Haram, D. Khushalani, *RSC Adv.* 2014, **4**, 17378.

Figure Captions

Figure 1. Schematic rational synthesis route for fabricating ultrathin PANI layers based on CNT/CNF template.

Figure 2. (A)-(C): SEM micrographs of purified CNFs, CNT/CNFs, and a typical CNT-grown CNF, respectively; (D): TEM image of CNT/CNFs.

Figure 3. (A) and (C): SEM micrographs of PANI/CNFs and PANI/CNT/CNFs, respectively; (B) and (D): TEM images of PANI/CNF and PANI/CNT/CNF, respectively.

Figure 4. (A): Raman spectra of CNT/CNF and PANI/CNT/CNF films; (B): FTIR spectra of CNT/CNF and PANI/CNT/CNF films, respectively.

Figure 5. (A): Nyquist plots of PANI/CNF and PANI/CNT/CNF film electrodes; (B): CV curves of stainless steel mesh, CNF, CNT/CNF, PANI/CNF, and PANI/CNT/CNF film electrodes at a scan rate of 5 mV s^{-1}; (C) and (D): CV curves of PANI/CNF and PANI/CNT/CNF film electrodes at varying scan rates, respectively.

Figure 6. (A): GCD curves of CNF, CNT/CNF, PANI/CNF, and PANI/CNT/CNF film electrodes at a current density of 0.3 A g^{-1}, respectively; (B): GCD curves of PANI/CNT/CNF film electrodes at different current densities; (C): Specific capacitance *vs.* current density for PANI/CNF and PANI/CNT/CNF film electrodes; (D): Charging/discharging cycling stability of PANI/CNT/CNF film electrodes at a current density 15 A g^{-1}.